Monte Carlo investigation of electron beam output factors versus size of square cutout

G. G. Zhang
Carleton University, and NRC, Ottawa, Canada

D. W. O. Rogers[a)]
National Research Council of Canada, Ottawa K1A OR6, Canada

J. E. Cygler
Ottawa Regional Cancer Centre, Ottawa, Canada

T. R. Mackie
University of Wisconsin, Madison, Wisconsin

(Received 18 March 1998; accepted for publication 25 February 1999)

A major task in commissioning an electron accelerator is to measure relative output factors versus cutout size (i.e., cutout factors) for various electron beam energies and applicator sizes. We use the BEAM Monte Carlo code [Med Phys. **22**, 503–524 (1995)] to stimulate clinical electron beams and to calculate the relative output factors for square cutouts. Calculations are performed for a Siemens MD2 linear accelerator with beam energies, 6, 9, 11, and 13 MeV. The calculated cutout factors for square cutouts in $10\times10\,\mathrm{cm}^2$, $15\times15\,\mathrm{cm}^2$, and $20\times20\,\mathrm{cm}^2$ applicators at SSDs of 100 and 115 cm agree with the measurements made using a silicon diode within about 1% except for the smallest cutouts at SSD=115 cm where they agree within 0.015. The details of each component of the dose, such as the dose from particles scattered off the jaws and the applicator, the dose from contaminant photons, the dose from direct electrons, etc., are also analyzed. The calculations show that in-phantom side-scatter equilibrium is a major factor for the contribution from the direct component which usually dominates the output of a beam. It takes about 6 h of CPU time on a Pentium Pro 200MHz computer to simulate an accelerator and additional 2 h to calculate the relative output factor for each cutout with a statistical uncertainty of 1%. [S0094-2405(99)01405-4]

Key words: electron beam dosimetry, relative output factors, cutout factors, Monte Carlo

I. INTRODUCTION

Commissioning of an accelerator for electron beam radiotherapy includes the measurement of many electron beam relative output factors versus field size and distance between the nominal source and the phantom surface (SSD). A cutout is an insert on the last scraper of the applicator, i.e., the part of the applicator closest to the phantom surface. Measuring the cutout factors, i.e., the relative output factors (ROF) versus cutout size, takes a lot of effort. There are many papers[1–4] that deal with the calculation of relative output factors, but in clinics, measurement is the most commonly used approach. This paper will show that Monte Carlo calculation is another option.

BEAM,[5] a Monte Carlo simulation code based on the EGS4 system,[6,7] is used here for the calculation of cutout factors. Our results show that this method is both accurate and practical for obtaining cutout factors. A unique advantage of the calculations is that they provide a detailed knowledge about components of the dose, such as the dose deposited in a phantom by the particles scattered off the applicator or the jaws, and/or by contaminant photons, etc. This provides a better understanding of the beam and the cutout factors.

This paper deals with square cutouts and defines the electron beam relative output factor as a function of cutout size, i.e., the cutout factor ROF(A), as the ratio of the dose per monitor unit at the depth of maximum dose, $d_{\max}$, for the field of interest to the dose per monitor unit of the reference field size at its own $d_{\max}$ (represented by $d_{\max 0}$), i.e.,

$$\mathrm{ROF}_{\mathrm{SSD}}(A)=\frac{(D/U)(A,\mathrm{SSD},d_{\max})}{(D/U)(A_0,\mathrm{SSD},d_{\max 0})}, \tag{1}$$

where D/U is dose per monitor unit, A is the field size, A_0 is the reference field size defined by the open applicator, and SSD is the distance between the nominal source and the phantom surface. Clinically, an SSD of 100 cm is often used. Sometimes, an SSD larger than 100 cm is used due to an anatomical restriction. Keep in mind that Eq. (1) applies, as we define it, to a given SSD. This is a slight extension of the definition of the output factor used by the AAPM's TG-25[8] where variation in SSD is allowed. We discuss variations with SSD extensively elsewhere,[9] but include results at a second SSD to demonstrate the ability to predict and explain the variations versus square cutout size at different SSDs (we use 115 cm because it is the second most commonly used SSD at the Ottawa clinic).

The scattered and direct components of electron beams are illustrated in Fig. 1. Those electrons that experience at least one scattering off field-defining components belong to the scattered component which has two subgroups: one scattered off the jaws, the other one off the applicator. Those

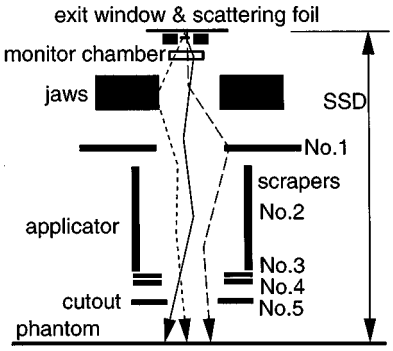

FIG. 1. A simplified schematic of an MD2 Siemens accelerator head and some typical electron beam paths. The long-dashed line represents an electron scattered off the applicator, the dashed line represents an electron scattered off the jaws, and the solid line represents the path of a direct electron. A cutout, if applicable, is inserted in the fifth scraper. The model used in the simulation is more realistic (see Fig. 2).

scattered only in the air, scattering foils, and monitor chamber, are defined as the direct component. Besides electrons, there are many contaminant photons created in the exit window, scattering foils or elsewhere in the accelerator head by electron bremsstrahlung. The number of photons at the phantom surface is often greater than the number of electrons, especially for high-energy breams and small fields. Every component of the dose behaves differently. In general, the direct component is the major source of the dose on the central axis. The component scattered off the applicator is very dependent on the cutout size, while that off the jaws is relatively constant. The contaminant photon component is dependent on energy and cutout size as well. All the scattered components and photon component together contribute less than 10% of the total dose at $d_{\max}$. We present a more detailed discussion on the dose contributions from the different components in the following sections.

II. MEASUREMENTS

The cutout factors are measured for a Siemens MD2 linear accelerator at the Ottawa Regional Cancer Center for electron beams with energies 6–13 MeV using an RFA 300 dosimetry system (Therados) with a Scanditronix Si *p*-type electron detector silicon diode. The active volume is 2.5 mm in diameter and 0.45 mm thick. A subset of cutout factors is also measured with an RK ion chamber (0.12 cc) to verify that the diode response is accurate. The measurements using the two detector systems agree with each other very well after stopping power ratio corrections[10] and polarity corrections are applied to the chamber readings (within 1% for all measured cutout factors except one case with a 2% discrepancy). These two detector systems were also compared for other measurements and they were in good agreement for all the comparisons conducted.[11] Measurement reproducibility for the silicon diode system is better than 0.5% and the overall uncertainty is estimated to be 1%. Given the agreement between the two systems, in this paper we report the relative output factor results using the diode. The % depth-dose curves and lateral profiles for each field size are also measured using the silicon diode.

The accelerator has various electron applicators with nominal source to applicator-end-distance of 95 cm. This introduces a 5 cm air gap between the applicator end and the standard SSD=100 cm plane. Square cutouts with thickness of 1.2 cm are inserted into applicators to define field sizes smaller than a given open applicator. The cutout is made of cerrobend, a bismuth(50.0% by weight)–lead(26.7%)–tin(13.3%)–cadmium(10.0%) alloy. In this paper, a $10\times10\,\mathrm{cm}^2$ applicator defines a field of $10\times10\,\mathrm{cm}^2$ at SSD=100 cm. The actual opening in the applicator is $9.5\times9.5\,\mathrm{cm}^2$. Similarly, the opening size of a $2\times2\,\mathrm{cm}^2$ cutout is actually $1.9\times1.9\,\mathrm{cm}^2$, a $3\times3\,\mathrm{cm}^2$ cutout is $2.85\times2.85\,\mathrm{cm}^2$, and so on.

III. SIMULATIONS

We use the BEAM code[5] to simulate the beams from an MD2 accelerator and the dose deposited in a water phantom. Usually, a complete simulation of an electron beam and the dose deposited in the phantom consists of two steps.

The first step is to simulate the transport of particles inside the accelerator head, and to create a phase-space file at the end of an applicator or just before the last scraper where the cutout is inserted. The accelerator head is composed of a series of component molecules (CMs) which represent the exit window, primary collimator, scattering foil, monitor chamber, *x* and *y* jaws, applicator, and so on. A monoenergetic electron pencil beam is incident on the exit window in the simulations discussed in this paper. A previous study by Ding *et al.*[12] showed that there is little difference in the depth-dose curve when using incident electrons which are either monoenergetic or have symmetric energy spectra. We start the simulation by selecting incident electron energies to match the measured values of R_{50} for the open $10\times10\,\mathrm{cm}^2$ applicator and use the selected energies to simulate beams with other applicators and cutouts. The incident electron energies at the exit window are usually higher than the nominal beam energies. For example, the incident energy for 11 MeV beam simulations is 11.95 MeV. However, at the surface of the phantom, the mean energy of the 11 MeV beam inside the $10\times10\,\mathrm{cm}^2$, field is about 10.5 MeV. For smaller beams the value of R_{50} decreases substantially. This is not due to the change of the mean energy in the beam, but is entirely an in-phantom effect. For example, the average energy in the $2\times2\,\mathrm{cm}^2$ 11 MeV beam is 10.6 MeV, even slightly larger than that of the $10\times10\,\mathrm{cm}^2$ field despite the fact that R_{50} decreases from 4.5 cm for the $10\times10\,\mathrm{cm}^2$ field to 3.6 cm for the $2\times2\,\mathrm{cm}^2$ field.

From the exit window, the particles travel in the geometry defined by the component modules. Figure 2 is an example of the simulation.

The simulation of the accelerator head creates a phase-space file which contains information about every particle in the scoring plane, including the energy, the position, the direction the particle is heading, as well as where it has been

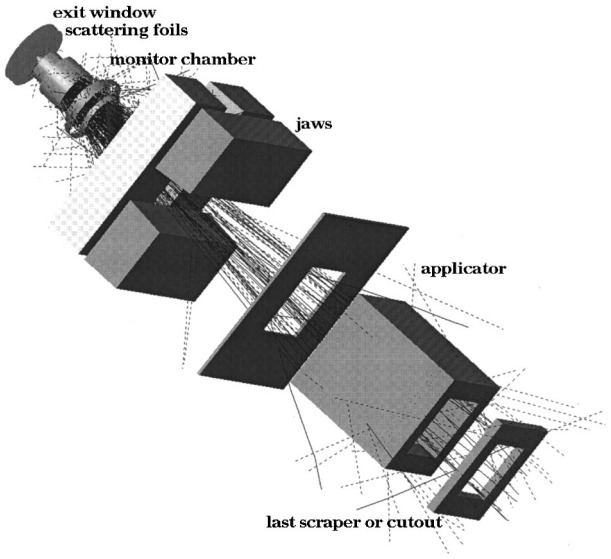

FIG. 2. The geometry of a Siemens MD2 accelerator head, and the simulated electron beam. The last scraper, corresponding to No. 5 in Fig. 1, where the cutout is inserted, is 5 cm above the phantom surface. Electrons are represented by solid lines while photons are dashed lines. In this example, there are 200 incident electrons with 10 electrons and 24 photons registered at the scoring plane which is at the phantom surface.

scattered, and where it has been created if applicable.[5] The phase-space file for the cutout factor calculation is output at a plane right before the cutout.

The second step is to use the phase-space file created in the first step to simulate the particle transport through the last scraper or cutout and in the phantom. In this paper, only square openings are discussed. We do the cutout simulation together with the dose deposition simulation in the phantom so that we can use the phase-space file for the rest of the accelerator simulation repeatedly for all the cutout sizes. The same phase-space file is also used in the calculations at extended SSDs. For an SSD of 115 cm, one just puts the phantom 15 cm further away and includes the extra air in the simulation.

For different cutouts, as long as the setting of the jaws and the applicator size are not changed, we find that the dose deposited in the monitor chamber per incident particle on the exit window is the same. Thus in the calculation of cutout factors, dose at $d_{\max}$ per incident particle is used as the beam output instead of dose per monitor unit.

In the phantom, the dose scoring volume along the central axis is set to be a cylinder with a radius of 5 mm. Using detailed dose profiles in a $2\times2\,\mathrm{cm}^2$ field at $d_{\max}$ indicates that averaging over a 1 cm diameter circle underestimates the dose on the central axis by less than 0.5% in this worst-case situation. For larger fields, the difference is negligible since the dose profiles at $d_{\max}$ are flat in the small area around the central axis. For large fields, a larger scoring volume can be used to improve statistics.

The simulation time is applicator size dependent. An accelerator simulation with a $10\times10\,\mathrm{cm}^2$ applicator takes about 6 h of CPU time on a Pentium Pro 200MHz machine to create about 1.4 million particles in the phase-space file which takes about 40 Mbytes of disk space. The second step for various cutout sizes takes about 1–2 h of CPU time. This typical phase-space file size for a large field gives statistical uncertainties on the dose at $d_{\max}$ of about 1%.

Uncertainties in the calculated dose are obtained by splitting all calculations into ten batches and estimating the uncertainty of any quantity from the variation in the results for each batch. This overestimates the uncertainty on the cutout factors which are obtained by assuming the calculated doses in the numerator and denominator are uncorrelated whereas they are strongly correlated since they are based on calculations with a common phase space file as the incident beam. Thus the statistical uncertainties on the calculated output factors are conservative upper limits.

IV. RESULTS

The depth-dose curves from calculations agree with measurements very well for all applicator and cutout sizes. These data have been presented previously.[10]

A. Cutout factors

Figure 3 shows the measured and calculated cutout factors for several different energies of electron beams for a $10\times10\,\mathrm{cm}^2$ applicator, at SSDs of 100 and 115 cm. Both curves in each plot are normalized to the open applicator which defines a $10\times10\,\mathrm{cm}^2$ field at SSD=100 cm or a $11.5\times11.5\,\mathrm{cm}^2$ field at 115 cm. The agreement between the measurements and the calculations is within about 1% except for the smallest cutouts at SSD=115 cm which agree within 0.015. The measurement data using the silicon diode system are used in this comparison. Similar agreement is found for data taken with the 15×15 and $20\times20\,\mathrm{cm}^2$ applicators (Fig. 4).

B. Side-scatter equilibrium

The concept of in-phantom side-scatter equilibrium is very important in understanding the variation in output from direct electrons. At the collimator level, if more than 99% of the particles that could reach the point of interest in the phantom pass through the collimator opening, then side-scatter equilibrium is said to exist.[8] In this paper, a 99% dose level is used instead of 99% of the particles because dose is a measurable quantity and we assume that dose at $d_{\max}$ is proportional to the number of particles passing through the collimator that could influence the dose at $d_{\max}$.

To study the variation of relative output factor and side-scatter equilibrium at $d_{\max}$ as a function of field size and energy, we simulated parallel monoenergetic electron beams of different energies incident on a water phantom with field sizes from 2 to 20 cm in diameter. Figure 5 shows that for a given beam energy there is a critical field size needed to establish side-scatter equilibrium at $d_{\max}$ in the phantom (Fig. 6). It is not necessarily true that as the energy increases the field size needed to reach side-scatter equilibrium at $d_{\max}$ is larger. Figures 5 and 6 show that as the field size increases, the 40 MeV beam reaches the 99% dose criterion before the 20 and 30 MeV beams do. Although high-energy beams

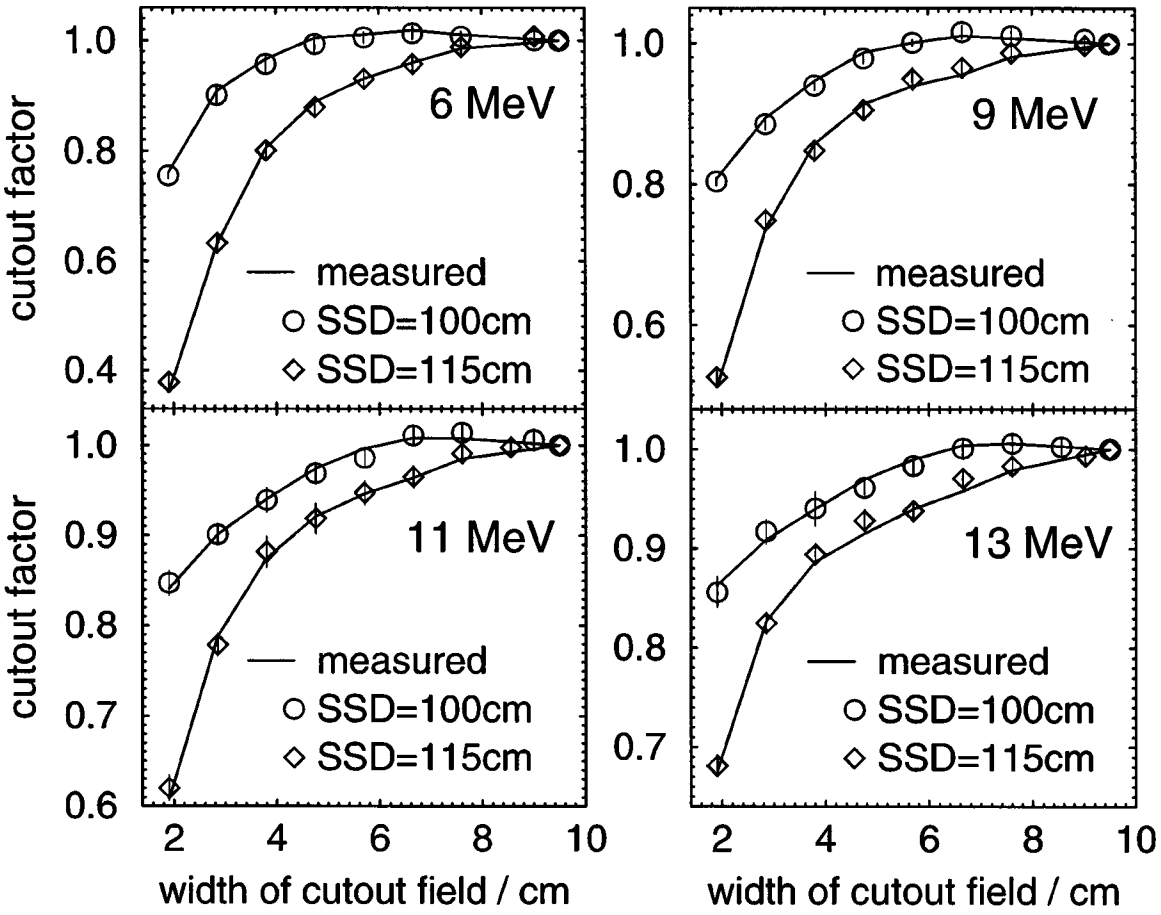

FIG. 3. Cutout factors for 6, 9, 11, and 13 MeV beams. The reference field is the open applicator which defines a 10×10 cm^2 field at SSD=100 cm. Note the different scales and the one standard deviation error bars. The measurements are performed using a silicon diode detector. The difference between the calculations and measurements is up to about 0.01 and within 1% for all except the smallest fields at SSD=115 cm.

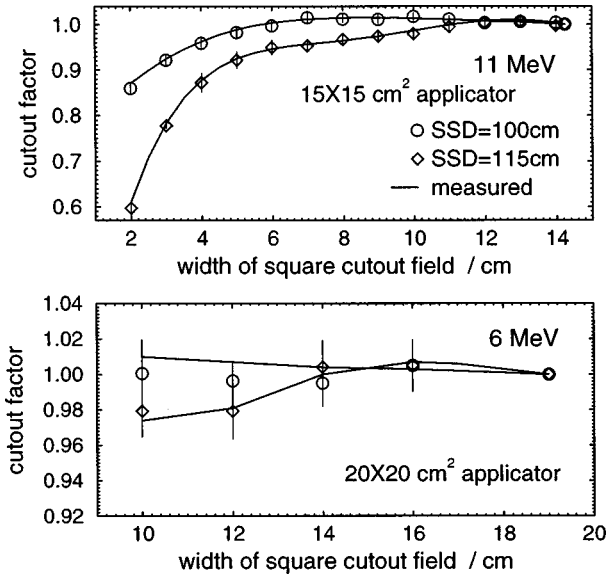

FIG. 4. Cutout factors for 11 MeV beams with a 15×15 cm^2 applicator and 6 MeV beams with a 20×20 cm^2 applicator. The reference fields are the open applicators. Note the different scales and the one standard deviation error bars. The difference between the calculations and measurements is up to about 1%.

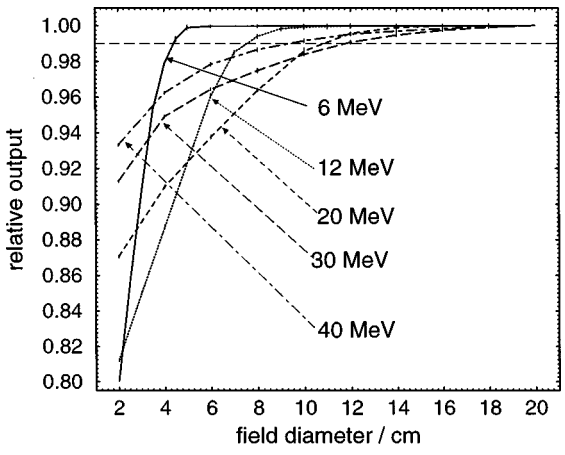

FIG. 5. Relative output at d_{max} for each beam versus circular field size for mono-energetic parallel electron beams. Each beam is incident from vacuum on a water phantom. For each energy, the output reaches a plateau. This means side-scatter equilibrium at d_{max} is established. The field size to establish side-scatter equilibrium at d_{max} is energy dependent. All the curves are normalized to their own outputs at a field diameter of 20 cm which is wide enough for all these energies to have side-scatter equilibrium at d_{max}. For a field with infinite radius the output of the beam is less than 0.1% larger than that of the 20 cm diameter field for all the energies.

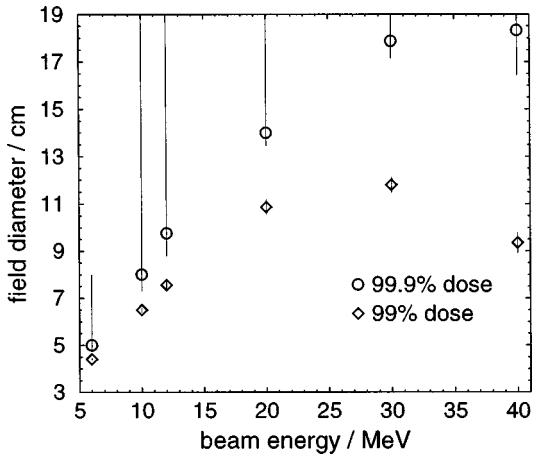

FIG. 6. Energy dependence of the field size to establish side-scatter equilibrium at d_{max} defined in terms of dose as a fraction of a broad beam dose. For the 40 MeV beam, the field size to establish side-scatter equilibrium at d_{max} is smaller than that of 20 and 30 MeV beams if 99% of dose maximum is the criterion. The upper error for the 99.9% dose curve is meaningless because the error bars on most dose calculations are larger than 0.1%.

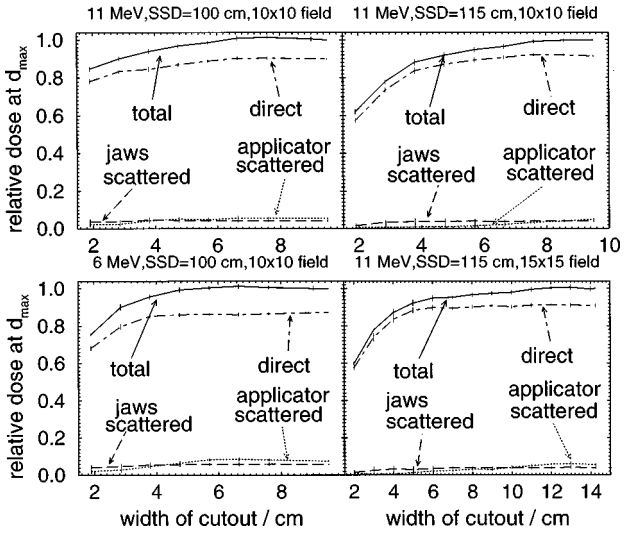

FIG. 7. Contributions of dose components to calculated relative output factors. The major change in the output versus cutout size comes from the direct electrons. For example, for the 11 MeV beam at SSD=100 cm, the total change is 10% between the open 10×10 and 3×3 cutout and 6.5% of this change is from the direct electrons. The scattered component from the jaws is relatively flat and the scatter from the applicator contributes a 3% change for the same beam. The decrease for smaller cutouts is greater at SSD=115 cm and more of the difference is due to direct electrons. The decrease for smaller cutouts is also greater for lower beam energies, but in this case the scattered components contribute more to the difference. All the curves are normalized to the total dose at d_{max} of each open applicator.

eventually scatter further laterally than low-energy beams, what Fig. 6 tells us is that at the depths of their respective dose maxima, the 40 MeV beam has not spread laterally as much as the 20 or 30 MeV beams. This is because the depth of dose maximum for the 40 MeV beam is much closer to the surface relative to R_{50} than for the other beams and the higher-energy beam has not spread out as much at that point as the lower-energy beams.

As long as side-scatter equilibrium at d_{max} is established, no matter how much wider the opening of the cutout is, the dose at d_{max} from the direct electrons will remain the same, i.e., it is a ''broad beam'' output.

C. Direct and scattered components

Figure 7 presents contributions from individual components of the dose output versus cutout size for several energies (6 and 11 MeV), applicator sizes (10×10 and $15\times15\,cm^2$) and SSDs (100 and 115 cm). In all cases, the difference between the output of the open applicator and the $2\times2\,cm^2$ cutout is mainly due to direct electrons, and, to a lesser extent, the particles scattered off the applicator.

Although the real beam is not a monoenergetic parallel beam as in Figs. 5 and 6, there is a critical cutout size beyond which side-scatter equilibrium at d_{max} exists for the direct electrons. The direct components of the ROFs in Fig. 7 reach a plateau as the cutout size increases.

This is not always true for the total dose. In both the measurements and calculations, as the cutout size increases at SSD=100 cm, the total output decreases slightly after it reaches its highest value (see Fig. 3 and SSD=100 data in Fig. 7). According to the definition, side-scatter equilibrium at d_{max} still exists with large cutouts. The decrease of the total dose with further increase of the cutout size is caused by a reduction in the dose component scattered off the applicator. The reason for the slight reduction is that many of the scattered particles are from the edge of the opening (Fig. 8).

As the cutout size increases, the edge of the cutout is getting further away from the central axis and thus many electrons scattered off the cutout, usually with low energy, can no longer reach the central axis at d_{max}. This component thus contributes less dose to the total dose at d_{max}. However, the dose from the direct electrons remains the same past the critical cutout size at which side-scatter equilibrium is established at d_{max}.

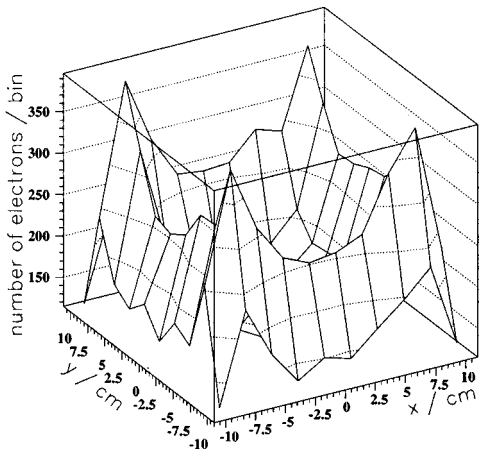

FIG. 8. Planar fluence distribution at the phantom surface of the electrons scattered from the last scraper, SSD=100 cm. The field size is $15\times15\,cm^2$. The energy of the beam is 11 MeV. Most of the electrons are from the edge of the scraper. This figure is obtained by analyzing the phase space output at the phantom surface by using PAW software (Ref. 14).

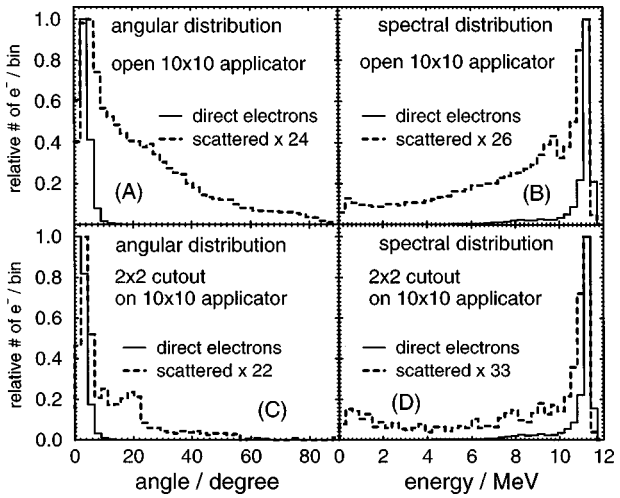

FIG. 9. Angular [(A) and (C)] and spectral [(B) and (D)] distributions inside the 11 MeV beam for an open applicator of 10×10 cm^2 [(A) and (B)] and 2×2 cm^2 cutout [(C) and (D)]. Most of the direct electrons go forward with high energy (the dip at 0° is a solid angle artifact). The lower-energy peak in the scattered electrons curve in (B) is created by electrons going through the first scraper. There are 40 equal bins in each curve. The scattered component is normalized to the peak of the direct component.

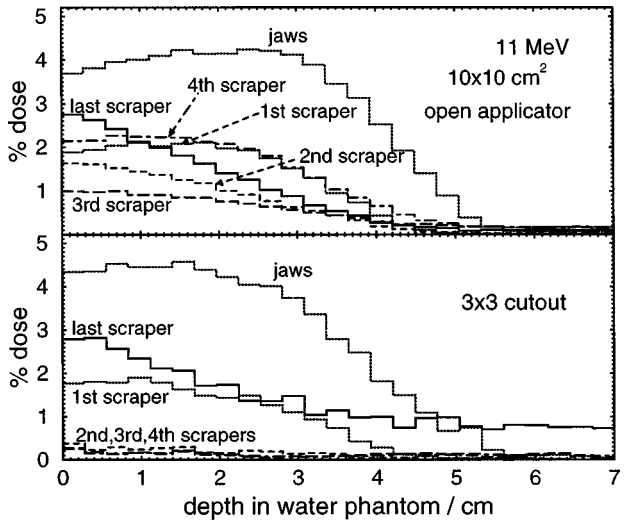

FIG. 10. Depth-dose curves for scattered components for 11 MeV beam, 10×10 cm^2 applicator, SSD$=$100 cm. Both cases are normalized to their own total dose at d_{max} which is 10% less for the 3×3 cutout case. Doses are from both electrons and photons. The numbering of the scrapers corresponds to Fig. 1.

Because the direct electrons undergo only multiple scattering in the air between the monitor chamber and the phantom, most of them have high energy and are going forward (Fig. 9). Both the angular and spectral distributions for the direct component do not change much with cutout size. For the scattered component, a small cutout stops many electrons scattered off other scrapers and these electrons tend to have a wide range of angles. Comparison of Fig. 9(A) with Fig. 9(C) shows that the cutout preferentially lets through those scattered electrons which are more forward peaked. The small peak at about 20° in Fig. 9(C) corresponds to the electrons from the second last scraper. Electrons at large angles are usually low in energy and these are stopped by the small cutout. Thus, in Fig. 9(D) for the 2×2 cm^2 cutout, the relative number of electrons with energy less than 10 MeV is lower than in the open field [Fig. 9(B)].

The direct component is about 90% of the dose at d_{max} for large fields, and even more for the small cutouts (Fig. 7). Usually, as the applicator (not cutout) size gets smaller, the fractional contribution from the direct component gets smaller due to the increased scatter from the jaws and applicator. This is not true when the change of the field size is made by changing cutout size. The reason can be seen in Fig. 10 which compares the depth-dose curves of the scattered components in a small field to those in a large field. When the cutout opening is small, the cutout stops many of the electrons scattered off the other scrapers while the fractional dose from the electrons scattered off the cutout does not change much. Thus the dose contribution from the scattered electrons decreases for the smaller cutouts (as seen in Fig. 7).

The setting of the jaws is not changed in the two fields shown in Fig. 10, and the jaws are far away from the cutout that sits in the last scraper. Thus the fractional dose from the jaw-scattered particles does not change much at d_{max}, although there is a small shift of d_{max} towards the surface in the small field. This shift is an in-phantom effect which matches that of the direct component. For the same reasons, the fractional dose from the first scraper also changes little. The dose components from the second, third, and fourth scrapers are significantly reduced by the small cutout which blocks many of the electrons from these scrapers which are going towards the central axis at a large angle.

At d_{max}, the scattered components are about 10% of the dose for the large fields. About half the scattered component dose comes from the jaws. The other half comes from the scrapers. For those fields smaller than 4×4 cm^2 at SSD$=$100 cm, the scattered component from the scrapers is less because of the blocking effect of the cutout.

Usually, the scattered components contribute only a few percent to the output. These components have lower energy than the direct component (see Fig. 9). Thus they contribute relatively more to the surface dose than to the dose at d_{max}, and move the d_{max} of the total depth-dose curve towards the surface (Fig. 11).

D. Contaminant-photon component

In the small field in Fig. 10, the dose from the cutout has a larger bremsstrahlung tail than in the large field. This is because there are many more high-energy electrons hitting the cutout in the small-field case, thus creating more photons that reach the phantom and contribute to this tail in the depth-dose curve. The photon tail from this component is less than 1% of the total dose at d_{max}.

The number of contaminant photons often exceeds the number of electrons for high-energy beams and small field sizes, but the dose contribution from photons is low and often negligible. The dose contribution from contaminant photons depends on energy and cutout size. The higher the

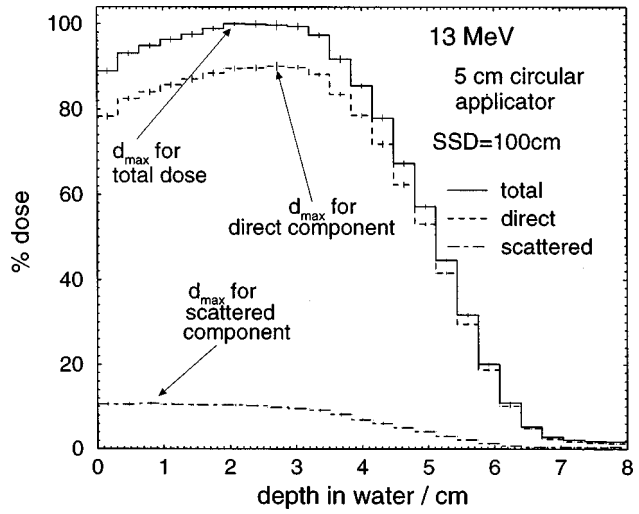

FIG. 11. Values of d_{max} for different components. With higher mean energy, the d_{max} for the direct component is deeper than that for the total while that for the scattered component is closer to the surface.

energy is, the higher the contaminant photon dose will be since bremsstrahlung is more likely with high-energy electrons. Also the contaminant dose is higher for smaller cutout sizes. Table I shows the dependence of the contaminant dose on the beam energy and cutout size for the $10\times10\,\mathrm{cm}^2$ applicator at SSD=100 cm. In the table, contaminant dose at d_{max} is normalized to the total dose at d_{max} of its own beam.

E. Sensitivity to accelerator model

At the time the calculations reported here were done our calculated applicator factors (relative output factors versus applicator size) differed from measurements by up to 5% while the cutout factors were calculated correctly within 1% as shown above. The problem for the applicator factor calculations was an extra component in the accelerator model which was outside the geometric beam and only blocked some widely scattered direct electrons from reaching the phantom. Since this component was only removing a few direct electrons, it had no effect on the central-axis depth-dose curves. With this extra component removed, the calculated applicator factors agree well with measurements and are reported in detail elsewhere together with calculations for circular, rectangular, and irregular fields.[13] We have confirmed that the extra component had no effect on the relative output factor calculations reported here by calculating a set of cutout factors without the extra component in place. There was no change in the cutout factors within the typical statistical uncertainty of 1% or less. Thus we present the extensive set of calculations which include this extra component.

This accidental mistake clearly demonstrates that calculated cutout factors are not very sensitive to some of the details in the accelerator simulation whereas the calculated applicator factors are far more sensitive to all of these details. This insensitivity of the cutout factors to the details of the accelerator model is also the reason that other algorithms, such as the SQRT and 1D methods of Mills *et al.*[1] can predict cutout factors based on known cutout factors without any geometry details.

TABLE I. Contaminant photon dose at d_{max} for open and small fields in 6 and 13 MeV beams for the Siemens MD2 accelerator

	6 MeV		13 MeV	
Beam	Open applicator	2×2 cutout	Open applicator	2×2 cutout
Photon dose	0.25%	0.72%	1.9%	3.1%

V. SUMMARY AND CONCLUSIONS

We have shown that Monte Carlo calculations for cutout factors agree with careful measurements within 1% except for the smallest cutouts at an SSD of 115 cm where the agreement is within 0.015. Thus Monte Carlo simulation can be an alternative to measuring ROFs versus cutout size in commissioning a clinical accelerator. Furthermore, it offers a powerful tool to better understand the related physics. The typical time to simulate an accelerator for a field of $10\times10\,\mathrm{cm}^2$ is about 6 h of CPU time on a Pentium Pro 200MHz machine and the dose distribution in a phantom takes about 1–2 h of CPU time for a statistical uncertainty of about 1%.

Side-scatter equilibrium is important to the direct component which dominates the total output. The output factor from the direct dose component plateaus once side-scatter equilibrium at d_{max} is established.

The scattered component, especially from the last scraper/cutout, is also important to the beam output. It contributes about 10% to the total output but tends to decrease for smaller cutouts.

The contaminant photon component contributes less than 1% to the total output for low-energy beams and about 3% for 13 MeV beams. As the cutout size decrease the photon contamination increases due to electrons giving off bremsstrahlung while stopping in the cutout.

Cutout factors are not as sensitive to the accelerator model as applicator factors are and the cutout factors can tolerate some small mistakes in the accelerator simulation. This suggests that Monte Carlo calculated values of cutout factors would be a good choice for the first routine use of Monte Carlo in clinical radiotherapy since measuring a complete set of cutout factors can take a long time.

ACKNOWLEDGMENTS

We would like to thank Jan Seuntjens, Iwan Kawrakow, Ken Shortt, Blake Walters, Daryoush Sheikh-Bagheri, Miller MacPherson, Michel Proulx, George Daskalov, Chunli Yang, Jette Borg, and Weihua Zhang, all at NRC, for helpful discussions and computer system support. We thank our former colleagues of NRC, George Ding, now of the Fraser Valley Cancer Center, and Charlie Ma, now of Stanford University, for helpful discussions. We thank Alfredo Siochi of

Siemens for very helpful mechanical data on the MD2 accelerator. This work was partially supported by NCI Grant No. R01CA52692.

[a]Electronic mail: dave@irs.phy.nrc.ca; WWW: http://www.irs.inms.nrc.ca/inms/irs/irs.html

[1]M. D. Mills, K. R. Hogstrom, and P. R. Almond, ''Prediction of electron beam output factors,'' Med. Phys. **9**, 60–68 (1982).

[2]M. D. Mills, K. R. Hogstrom, and R. S. Fields, ''Determination of electron beam output factors for a 20-MeV linear accelerator,'' Med. Phys. **12**, 473–476 (1985).

[3]I. A. D. Bruinvis and W. A. F. Mathol, ''Calculation of electron beam depth-dose curves and output factors for arbitrarily large fields,'' Radiother. Oncol. **11**, 395–404 (1988).

[4]B. J. McParland, ''A method of calculating the output factors of arbitrarily shaped electron fields,'' Med. Phys. **16**, 88–93 (1989).

[5]D. W. O. Rogers, B. A. Faddegon, G. X. Ding, C. M. Ma, J. Wei, and T. R. Mackie, BEAM: A Monte Carlo code to simulate radiotherapy treatment units, Med. Phys. **22**, 503–524 (1995).

[6]W. R. Nelson, H. Hirayama, and D. W. O. Rogers, ''The EGS4 Code System,'' Report SLAC-265, Stanford Linear Accelerator Center, Stanford, CA (1985).

[7]W. R. Nelson and D. W. O. Rogers, ''Structure and Operation of the EGS4 code system,'' in *Monte Carlo Transport of Electrons and Photons*, edited by T. Jenkins, W. Nelson, A. Rindi, A. Nahum, and D. W. O. Rogers (Plenum, New York, 1989) p. 287–306.

[8]F. M. Khan, K. P. Doppke, K. R. Hogstrom, G. J. Kutcher, R. Nath, S. C. Prasad, J. A. Purdy, M. Rozenfeld, and B. L. Werner, ''Clinical electron-beam dosimetry: Report of AAPM Radiation Therapy Committee Task Group 25,'' Med. Phys. **18**, 73–109 (1991).

[9]G. G. Zhang, D. W. O. Rogers, and J. E. Cygler, ''Monte Carlo study of variation of electron beam output with size of air gap,'' submitted to Med. Phys. (1998).

[10]G. G. Zhang, D. W. O. Rogers, J. E. Cygler, and T. R. Mackie, ''Effects of changes in stopping-power ratios with field size on electron beam ROFs,'' Med. Phys. **25**, 1711–1724 (1998).

[11]G. X. Ding and J. E. Cygler, ''Measurements of electron beam peak scatter factors,'' Med. Phys. **25**, 251–253 (1998).

[12]G. X. Ding, D. W. O. Rogers, and T. R. Mackie, ''Calculation of stopping-power ratios using realistic clinical electron beams,'' Med. Phys. **22**, 489–501 (1995).

[13]G. G. Zhang, D. W. O. Rogers, and J. E. Cygler, ''Monte Carlo calculations of electron beam output factors for arbitrary fields,'' submitted to Med. Phys. (1998).

[14]R. Brun, O. Couet, C. Vandoni, and P. Zanarini, ''PAW User Guide,'' CERN Computer Center, Geneva, Switzerland (1992).